

INTAR: Inter-Task Auto-Reconfigurable Accelerator Design for High Data Volume Variation in DNNs

Zifan He*, Anderson Truong*, Yingqi Cao[†] and Jason Cong*

*University of California, Los Angeles

Email: zifanhe1202@g.ucla.edu, andersonleetruong@gmail.com, cong@cs.ucla.edu

[†]University of California, San Diego

Email: yic033@ucsd.edu

Abstract—The rise of deep neural networks (DNNs) has driven a boom in AI services, which results in an increased demand for computing power and memory. In modern DNNs, the data sizes produced and consumed are highly varied across operations (high data volume variation, HDV). Because existing design paradigms use fixed execution patterns that lead to either low computational efficiency due to pipeline stalls or frequent off-chip memory accesses to manage large intermediate data, HDV applications are challenging to accelerate on FPGAs. To address these challenges, we introduce the Inter-Task Auto-Reconfigurable Accelerator (InTAR), a novel accelerator design for HDV applications on FPGAs. InTAR combines the high computational efficiency of sequential execution with the reduced off-chip memory overhead of dataflow execution. It switches execution patterns automatically with a static schedule determined before circuit design based on resource constraints and model parameters. Unlike previous reconfigurable accelerators, InTAR encodes reconfiguration schedules during circuit design, allowing model-specific optimizations that allocate only the necessary logic and interconnects. Thus, InTAR achieves a high clock frequency with fewer resources and low reconfiguration time. Furthermore, InTAR supports high-level tools such as HLS for fast design generation. We implement a set of multi-task kernels in various HDV DNNs using InTAR. Compared with dataflow and sequential accelerators, InTAR exhibits $1.8\times$ and $7.1\times$ speedups correspondingly. We also implement InTAR for GPT-2 medium as a more complex example, which achieves a speedup of $3.65 \sim 39.14\times$ and a $1.72 \sim 10.44\times$ boost in DSP efficiency compared to the corresponding SoTA accelerators (Allo and DFX) on FPGAs. Additionally, this design demonstrates $1.66 \sim 7.17\times$ better power efficiency than GPUs.

I. INTRODUCTION

The development of deep neural networks (DNNs) has driven numerous breakthroughs in AI-assisted applications [13], [14] while intensifying demands for compute efficiency due to increasing network complexity and memory requirements. As DNN applications grow in size [30], [34], larger data volumes generated during operations strain hardware resources during deployment. Consequently, a key challenge in designing DNN accelerators is: *Given resource constraints imposed by physical hardware limitations or power considerations, how can execution scheduling be improved to minimize end-to-end latency while accounting for hardware overhead?*

A common strategy of DNN accelerator designs is grouping computations belonging to the same matrix/vector operation into a **task** and scheduling computations at the task level. For example, self-attention [35] of transformer models involves

two tasks: QK^T and softmax operation. Previous accelerators focus on two types of fixed task execution patterns: **dataflow** (also called spatial) [6], [9] or **sequential** (also called temporal) executions [5], [24], [27], [43]. For **dataflow** executions, each processing element (PE) specializes in a single task. Data is streamed through FIFOs connecting PEs for dependent computations with minimal on-chip buffer for data reuse. Depending on the dataflow graph, it includes both task-pipeline and task-parallel executions. **Task-pipeline** streams data between dependent tasks, and **task-parallel** executes independent tasks in parallel. For **sequential** executions, a versatile PE processes tasks serially and parallelizes the computations inside each task. Resources are reused across operators. Although both execution patterns exhibit strong performance, each of them faces a major challenge for large DNN applications [8], [45]:

- **Dataflow: reduced computation resource efficiency.** Due to the coarse and fine-grained pipeline stalls from the data dependencies, some PEs in dataflow execution may remain idle, leading to low computation resource efficiency and high end-to-end latency.
- **Sequential: high off-chip memory access overhead.** Output data from previous tasks will be stored and reused by the next tasks in sequential execution. Moreover, data may be cached and remain unused until the consumer tasks start executions. Due to the limited on-chip resources, it is often difficult to store output data on SRAM. If storing data in the off-chip memory, the accelerator will suffer from high latency and energy consumption of off-chip memory access.

TABLE I
MINIMUM AND MAXIMUM INTERMEDIATE DATA SIZE OF SAMPLE DNNs

Model	Type	Min Data Size	Max Data Size
GPT 2 [29]	Transformer	$64L$	$\max(4096L, L^2)$
Llama 2 7B [34]	Transformer	$128L$	$\max(22016L, L^2)$
ResNet-50 [22]	CNN	151K	802K
ResNet-152	CNN	151K	802K
ResNext-101 [39]	CNN	151K	1.04M

To address both challenges simultaneously, we observe another commonly neglected feature of DNNs to exploit: **high data-volume variation** (HDV). Table I lists a set of DNN applications and the minimum/maximum input/output data size. L is the sequence length for transformer models. These models offer both a large maximum data size (up to 88 MB with $L = 2048$) and a significant data size variation

($5.3\times \sim 172\times$ from minimum to maximum data size). This indicates a potential solution to improve computation resource efficiency while circumventing off-chip memory access for intermediate data: executing sequentially for tasks producing small data within on-chip memory capacity, and stream data for tasks producing large data.

Therefore, we propose a novel accelerator design paradigm on FPGAs: **inter-task auto-reconfigurable accelerator** (INTAR). INTAR can switch execution patterns automatically based on on-chip memory and computation resources. When a task produces large intermediate data, INTAR pipelines multiple tasks to avoid accessing off-chip memory for these data. Otherwise, INTAR will process tasks sequentially to maximize compute efficiency by eliminating pipeline stalls. Compared with other reconfigurable accelerators [4], [7], [10], [25], [26], INTAR allows *model-specific circuit optimization* that keeps only necessary control logics and interconnects. Hence, INTAR requires fewer reconfiguration resources, achieves a high clock frequency, and low reconfiguration overhead (10 to 20 ns) (Section III). Since computations are reconfigured at the task level, INTAR is one of the first works regarding FPGA-based reconfigurable accelerators that support high-level hardware generation tools such as High-Level Synthesis (HLS) [11] for fast accelerator design. Our contributions include:

- We present INTAR, a novel accelerator design paradigm on FPGAs that balances the memory access and computational efficiency tradeoff for HDV applications (Section III).
- We illustrate the techniques to design INTAR with HLS and important considerations in placement and routing for hardware implementation of INTAR on FPGAs (Section IV).
- Evaluations. We implement INTAR for five multi-task kernels that broadly exist in DNN applications (Self-Attention, Multi-layer CNN, FFN layer, VAE, and Gating Network) to show its advantages. INTAR exhibits $1.8\times$ and $7.1\times$ speedup compared with the corresponding dataflow and sequential accelerator. We further present INTAR on the GPT-2 medium model for a complete DNN example, which achieves a speedup of $3.65 \sim 39.14\times$ and a $1.72 \sim 10.44\times$ improvement in DSP efficiency compared to the SoTA accelerators (Allo [9] and DFX [23]). Moreover, INTAR demonstrated $1.66 \sim 7.17\times$ better power efficiency compared to GPUs.

II. BACKGROUND AND MOTIVATIONS

A. Dataflow and Sequential DNN Accelerators

Dataflow accelerators allocate resources for each task in the DNN and pipeline the computations to save memory while maintaining performance. FlexCNN [6] is a framework for composing CNN-based DNN accelerators in HLS, and GenGNN [3] is a framework for GNN acceleration. Allo [8], [9] is a composable framework for designing accelerators on FPGA by parsing Python/Pytorch scripts and generating the corresponding HLS code for FPGAs for every operator. Accompanied by proper customization primitives, Allo can automatically combine the optimizations across different layers for a complex model.

On the other hand, sequential accelerators process layers in DNN sequentially and attempt to utilize all available resources. GPUs and TPUs [24] are considered instruction-based sequential accelerators that support various DNNs. ZyncNet [18] is a CNN accelerator deployed on Zync SoC with a specialized topology. FQ-BERT [27] is a sequential FPGA design for a fully quantized BERT model [12]. FlightLLM [42] is a vector processor implemented on Alveo U280 FPGA for Llama model inference.

B. Hybrid Accelerators

Previous works attempt to mitigate the drawbacks of dataflow and sequential accelerators by having a hybrid execution pattern. A naive approach is allocating part of the resource for dataflow execution and the rest for sequential execution [43]. A more recent method is to allocate several PEs and schedule multiple tasks to the same PE. For instance, SSR [45] is a hybrid accelerator implemented on AMD Xilinx Versal ACAP devices for vision transformers. By reserving two groups of AI engines for two types of matrix multiplies, SSR allows sequential executions of GEMMs to minimize latency and enables data forwarding between dependent GEMMs to reduce the memory cost. However, PE specializations of hybrid accelerators impede the flexibility of execution pattern switching, which may lead to stalls. Section II-E will further discuss the inefficiency of hybrid accelerators with an example.

C. Reconfigurable Accelerators

A reconfigurable accelerator can change its microarchitecture on the fly. A common implementation of such accelerators is the coarse-grain reconfigurable array (CGRA) [10], [26], [31], which compiles a dataflow graph into a configuration and modifies switches connecting PEs accordingly. However, CGRA has complex reconfiguration logic to ensure generalizability. This introduces area overheads [32] and additional wiring that negatively affects the timing [26].

An alternative method to reconfigure resources is dynamic partial reconfiguration (DPR) [38], which reserves regions on FPGAs to load partial bitstream for runtime reconfiguration. While having a low resource overhead for the configuration controller, it has a higher reconfiguration overhead (10 to 100 ms) than FPGA-based CGRA (around 10 ns).

Other reconfigurable accelerators focus on optimization under only specific computation scenarios [4], [7], [33]. For example, SET [7] performs inter-layer scheduling of convolution networks onto the tiled accelerators utilizing a time-space resource-allocation tree. FEATHER [33] mainly resolves reduction efficiency in each CNN layer by reconfiguring the reduction dataflow.

Considering these drawbacks, existing reconfigurable accelerators can hardly apply to a broad range of modern DNNs, which necessitates the development of a new design paradigm.

D. Applications with High Data Volume Variation

A multi-task application is defined as high data-volume variation (HDV) if the input/output data sizes between tasks are highly varied. Many of DNNs are HDV for two reasons:

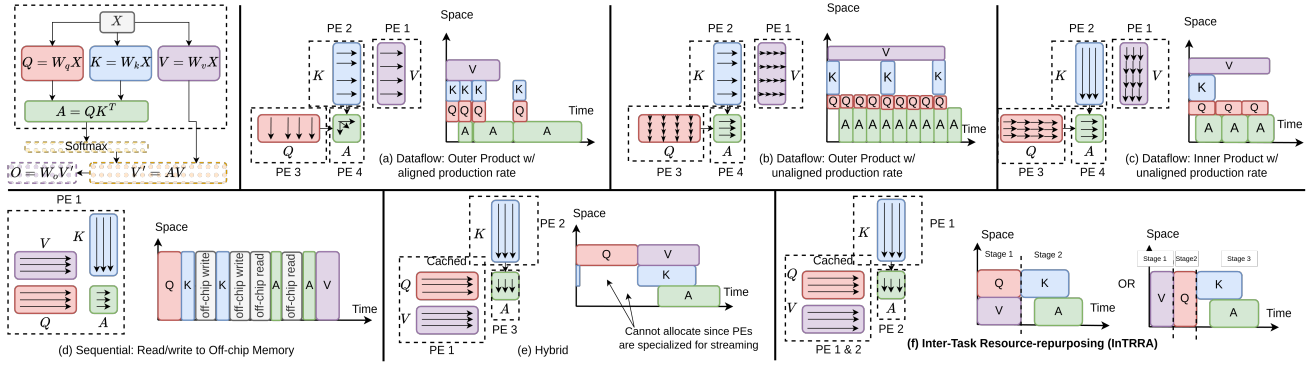


Fig. 1. Example of mapping computations of attention and linear projection of value matrix to the dataflow, sequential, hybrid accelerators, and INTAR. Depending on the scheduling of the rest of the computations in the entire model, INTAR can choose between task-parallel (left) and sequential modes (right) for better locality. Both will have the same latency.

- Modern DNNs have complex dependencies. Data is produced several layers ahead and can only be discarded after they are reused. Hence, the data production and elimination rates are largely varied.
- The objectives of many DNN workloads involve feature extraction (e.g., classification) that reduces the data size, or data construction (e.g., image/text generation) which increases the data size. By the nature of these workloads, the data size will change during execution.

E. Motivating Case Study: Attention + Linear Projection

We provide a case study to illustrate the advantages of inter-task reconfiguration for HDV DNNs: calculating the attention score and a linear projection of the value matrix. Figure 1 shows the dataflow graph of the attention layer and the timeline for each execution pattern. The direction of the arrows indicates the output production order and lengths represent the production rate. Here we focus on calculating Q , K , V , and A in the dashed square. In this example, we assume that:

- Matrix multiplies are weight stationary as weights are already stored on on-chip memory.
- Outputs (A and V) will be written into off-chip memory.
- The rest of the on-chip memory size will only store either Q or K , but not both.
- Input sequence is short, which means A can be stored in on-chip buffer with K or Q .

The pattern of data size variation is *first increase then decrease*. Dataflow execution instantiates PEs for each task. There are three ways to stream and cache data across tasks illustrated in Figure 1: outer product with aligned and unaligned production rates of Q and K , and inner product with unaligned production rates. Inner products with aligned production rates require caching of both Q and K , which is infeasible. Each case incurs compute resource idling due to either varied workload size of A (Figure 1(a)), back-pressure (Figure 1(b)), or early completion (Figure 1(c)).

Sequential execution instantiates a single PE to execute each task serially, as shown in Figure 1(d). Due to insufficient on-

chip memory capacity, it needs to read from and write to the off-chip memory, increasing the overall latency.

Some hybrid accelerators [45] can mitigate the issues by executing Q and V sequentially and pipeline K and A . However, since PEs are specialized for either streaming data or cached buffer [45], computation of V cannot be assigned to PE 2 and PE 3, and these two PEs are idle at the beginning, waiting for the arrival of data for Q .

For INTAR (Figure 1(f)), PEs can be reconfigured to either sequential or dataflow execution at different times. Therefore, PEs can be efficiently allocated while off-chip memory access for intermediate data is avoided. Section III discusses how INTAR manages this in detail.

III. INTER-TASK AUTO-RECONFIGURABLE ACCELERATOR

To improve resource efficiency, INTAR minimizes off-chip memory access by employing dataflow execution when necessary while keeping the rest of the execution as sequential as possible. The finest granularity of execution pattern switching is the **task**, which represents a group of computations belonging to the same matrix or vector operation. Execution pattern switching is achieved through automatic reconfiguration based on instructions stored in the static configuration buffer (Section III-B), which is hardened into the design. These instructions trigger computation behavior and data movement changes.

Unlike other reconfigurable [7], [10], [25], [26], [33] and overlay accelerators [40], [41], which prioritize abstraction and fast compilation, InTAR focuses on reconfiguration for optimization. The reconfiguration schedule in InTAR is determined at **circuit design time** rather than relying on post-design external commands. For every application, a **static schedule** is created based on the specific application and resource constraints, and the circuit is then tailored accordingly. This approach reduces reliance on general-purpose control units and cross-bars, retaining only essential reconfiguration logic and interconnects. The result is low resource utilization for reconfiguration controls (49% LUT reduction for a design with $3\times$ throughput compared to [26] for multiple GEMMs), high clock frequency ($2.41\times$ that of [26]), and low reconfiguration latency ($10^6\times$ faster than DPR [25], comparable to [26])

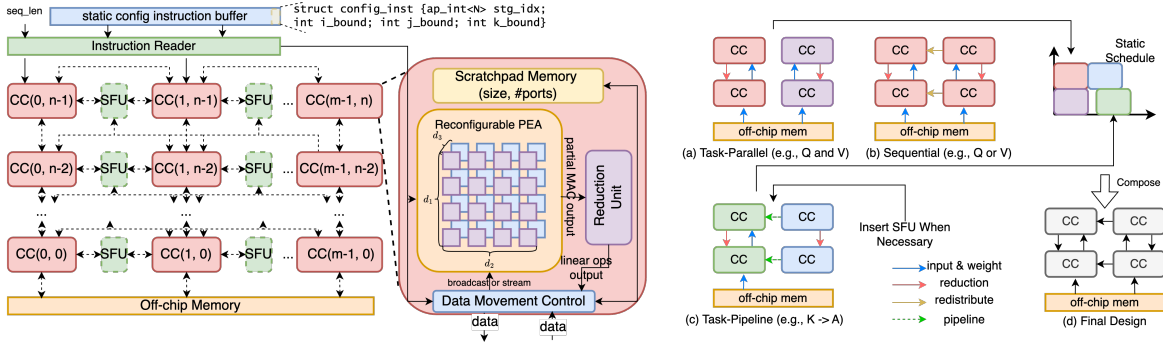


Fig. 2. Left: Architecture template of INTAR. Compute cores (CC) compute linear operations (e.g., GEMM, ConvNet), and SFUs compute non-linear operations (e.g., softmax, GeLU). Each CC contains a scratchpad memory, a reconfigurable MAC unit array, a reduction unit, and a data movement control unit. Dashed lines indicate the candidates for connection between CCs and SFUs. Right: example architectures for each execution mode within the template, with $n, m = 2$. For a schedule, we will compose the architectures of required modes to keep only necessary interconnects and logic.

TABLE II

COMPARISON BETWEEN INTAR AND OTHER DNN ACCELERATION WORKS. THE MAJOR REASON FOR HAVING IDLE COMPUTE RESOURCES IS DESCRIBED IN THE PARENTHESES FOR EACH WORK.

Prior works	Platform	Contribution Type	Accelerator Category	Inter-task Schedule	Idle Compute Resource Exist? (dataflow execution)	Intermediate Data Movement	When Reconfig Determined	Reconfiguration Design Scope	Model-spec. Design Opt.
Allo [9]	FPGA	Domain-Spec. Lang.	Dataflow	\times	Yes (dataflow execution)	On-chip only	-	-	\times
FQ-BERT [27]. DFX [23]	FPGA	Accelerator	Sequential	\times	No	On-/Off-chip	-	-	\times
SSR [45]	FPGA	Accelerator	Hybrid	\checkmark	Yes (PE specialization)	On-chip only	-	-	\times
FPCA [10], OverGen [26]	FPGA	Architecture	Reconfigurable	\times	Yes (single DNN)	On-/Off-chip	After circuit generation	General	\times
FEATHER [33]	FPGA	Accelerator	Reconfigurable	\times	No	On-/Off-chip	After circuit generation	Reduction Network	\times
SET [7]	ASIC	Scheduler	Reconfigurable	\checkmark	Yes (sub-opt. sched.)	On-/Off-chip	N/A	Tiled Accelerator	\times
INTAR	FPGA	Design Paradigm	Reconfigurable	\checkmark	No	On-chip only	Circuit design time	General	\checkmark

compared with FPGA-based CGRA and DPR approaches. Additionally, InTAR handles reconfiguration at the task level, enabling rapid and convenient development with high-level tools like HLS. This makes InTAR well-suited for FPGAs to adapt quickly to new DNN applications. Lastly, InTAR’s reconfiguration scope is not limited to specific computations. Table II compares InTAR with prior DNN accelerator works.

A. Execution Modes of INTAR

Depending on the available resources on FPGAs and the properties of tasks, INTAR configures the resources into sequential, task-pipeline, or task-parallel mode, corresponding to the dataflow and sequential execution patterns mentioned in Section I.

- **Sequential:** All resources perform a single task in parallel.
- **Task-pipeline:** Same as dataflow execution with pipelined dependent tasks. Computational resources are partitioned proportional to the workloads. Data are streamed from one task to another using FIFOs.
- **Task-parallel:** Same as dataflow execution with independent tasks running in parallel. The resource efficiency is the same as the sequential mode, but it may have a better locality for subsequent tasks (e.g., in Figure 1, if calculating AV and O are pipelined, then running Q and V in parallel and assigning V to the PE that will compute AV avoids data aggregation overhead from other PEs).

Figure 1(f) illustrates the task assignment and timeline of INTAR for the case study in Section II-E. PEs 1 and 2 handle both attention computation and linear projections. Depending

on the subsequent operations, INTAR can choose either task-parallel or sequential mode for Q and V . If the scheduler decides to serialize computing AV and O , then the sequential mode is more suitable to allow PEs 1 and 2 to execute cooperatively. If the scheduler pipelines computations of AV and O , then task-parallel mode is preferred to improve locality. Both choices will not affect the latency but determine the data movement overhead of the following tasks. After calculating Q and V , INTAR switches to task-pipeline mode to compute K and A , since storing Q consumes all scratchpad memory.

B. Architecture Template

Figure 2 is the architecture template of INTAR for HDV DNN applications, which consists of a grid of compute cores (CC) computing linear operations and special function units (SFU) inserted in between. Each CC contains:

- **Reconfigurable PE Array:** a multi-dimensional array of PEs that allow changing inputs and precisions. Connected in either a systolic array or broadcasting the data to all PEs. Each PE produces the complete or partial result of the linear operation.
- **Scratchpad Memory:** store intermediate and weight data.
- **Reduction Unit:** read the partial outputs from the PEA if needed and perform accumulations.
- **Data Movement Control Unit:** determine the flow of data to the scratchpad memory and other CCs/SFUs.

When switching execution modes, a global instruction reader will read both the configuration instructions from a static buffer and the input size passed as the kernel argument. It will then modify part of each instruction related to the input

size (e.g., the loop bounds) and send it to the CCs. The reconfigurable PEA and data movement control will read the instructions and propagate among the CCs. The instruction sequence is determined by the static schedule of mode switching at the circuit design time. Each instruction contains a **stage index** and several **loop bounds** (e.g., reconfiguring the three loop bounds for GEMMs). A stage refers to an execution of a single or a group of tasks that follows one of the execution modes, seen in Figure 1(f), e.g., computing Q and V in stage 1 and K and A in stage 2. Each CC has a specified behavior for each stage, orchestrated by multiplexers with stage indices as the select signals. Notice that the stage-to-behavior correspondences are specific for each application. Thus, INTAR only needs to handle the reconfigurations defined in the schedule. The reconfiguration overhead consists of four parts: reading, modifying, sending, and decoding instructions to generate signals for multiplexers in the CCs. Each of these is a single-cycle operation. Thus, reconfigurations have a 4-cycle overhead (10 to 20 ns depending on frequency).

The template has several design parameters for users to derive a specific architecture, including:

- Number of rows n and columns m of the CCs.
- Instantiation of the SFUs, which determine the positions and computations of each SFU.
- FIFO connections between the CCs and SFUs.
- Scratchpad memory size and number of memory ports.
- Reconfigurable PE array dimensions.

Depending on the schedule, we assign values to these parameters to perform the three execution modes mentioned in Section III-A. The right of Figure 2 depicts the example architectures of each execution mode derived from the template for $n, m = 2$ for the case study in Section II-E. The colors of connections indicate the purpose of communications (read input and weights, perform reductions, redistribute output, or pipeline intermediate results). For a specific schedule, we compose the derived architectures of the execution modes utilized to get the final circuit design. **Common interconnections and control logic across execution modes will be merged, and unused interconnects will never be introduced.**

IV. DESIGNING ACCELERATORS IN INTAR

A. Finding Schedule and Architecture Template Parameters

The development of INTAR for a new application starts with creating the static reconfiguration schedule. In this work, we first topologically sort the tasks based on dependencies in the dataflow graph and create the schedule based on the data size and resource constraints, using the following heuristics:

- If the total size of output and previously cached data is larger than the memory constraint, then select the task-pipeline mode.
- Otherwise, if task-parallel mode can improve locality for the subsequent tasks as illustrated in Section III-A, then pick task-parallel mode. If not, then choose the sequential mode.
- Non-linear operations are pipelined with previous tasks.

Then, we analyze the generated schedule and the hardware configurations and determine architecture template parameters

with the following heuristics: The schedule infers the instantiation of the SFUs and FIFO connections. The column count of CCs equals the maximum number of tasks of all stages, and the row count is the number of dies on the FPGA necessary to improve floorplanning. We compute the PEA dimensions to maximize utilization with limited cross-die communications and calculate the memory ports needed. Finally, the scratchpad memory is the maximum memory size required over all stages. Although the heuristics are not guaranteed optimal, we show that our schedule results improved performance consistently (Sections V, VI). We leave the development of an optimized DSE engine as future work.

B. Designing Reconfigurable Modules: A Case Study in HLS

Following the architecture template, there are three types of reconfigurations: data movement, compute, and control. All of them can be implemented in HLS efficiently with **conditional dataflow**, which utilizes if-else statements to declare the behavior changes and exploit HLS’s resource binding pass to merge interconnects and logic as much as possible.

Data Movement Reconfiguration: a majority of auto-reconfigurations in INTAR are powered by data movement control. In different stages, each CC may load data from various sources (e.g., other CCs, on-chip buffers, registers, or constants) and send it to multiple destinations. Figure 3 is an example of the data movement control reconfiguration in CC3: data flow from CC1 to buf 1 at stage 0 and flow from buf 2 to CC 2 at stage 1. The corresponding HLS code is a realization using the stage index as the condition to identify which flow the data movement control should adopt. Different stages can share data sources and destinations, which can potentially save interconnects. For instance, if the data flows from CC1 for each stage, the reader module can be reused.

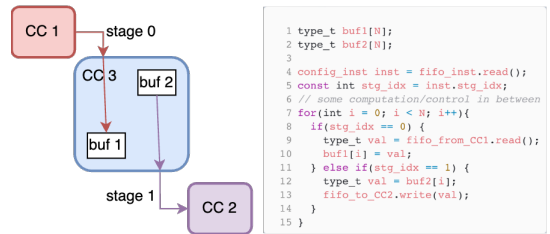


Fig. 3. Example of data movement reconfiguration. Left: In different stages, PE 3 either read from PE 1 and write to on-chip buffer buf 1, or read from buf 2 and write to PE 2. Right: the corresponding HLS code.

Compute Reconfiguration: Based on the definition of the architecture template, the reconfigurable PEA can change the input operands and the precision. Figure 4 illustrates a PEA switching the data source between stages, where each source is interpreted as a different precision. To change the input operands, we adopt a similar method of data movement reconfiguration to extract inputs from two source buffers conditioned on the stage index. Inputs are packed for data parallelism. Then, when computations start, each PE will select part of the input operand and pad with zeros to make sure the bitwidths are uniform across stages. This guides the HLS to

bind compute resources between stages. The two steps cannot be merged, otherwise the HLS will instantiate two PEAs with different precision specifications.

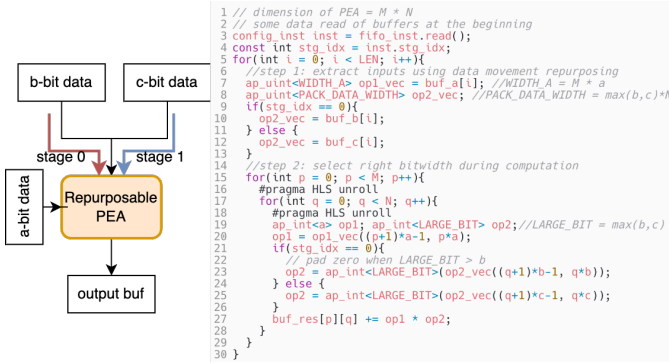


Fig. 4. Example of compute reconfiguration. Left: The reconfigurable PEA consumes different buffers at each stage and supports mixed precision of b-bit and c-bit calculations. Right: the corresponding HLS code.

Control Reconfiguration: In INTAR, there are control reconfigurations for loop bounds and data-dependent conditional dataflow. For loop-bound control, we can implement variable loop bounds for different stages of computations using the configuration instructions (left of Figure 5). For data-dependent conditional dataflow, when the behavior of executions depends on both stage index and other data sources, we can compose the conditions with logical operators (right of Figure 5).



Fig. 5. Example of control reconfigurations in HLS. Left: loop bound control. Right: data-dependent conditional dataflow.

All accelerators in the INTAR paradigm are covered by the compositions of these three types of reconfigurations, indicating complete support in HLS.

C. Important Considerations in Placement and Routing

In order to achieve rapid development, we need to make sure that the generated design is both valid and performant. Following are several important considerations of implementing a place-able and routable INTAR design with high frequency. **Distribute Independent Tasks Across Dies.** For multi-die FPGAs [1], [2], cross-die wires are limited and often negatively affect the timing. Thus, when encountering a design with resource utilization higher than the single-die capacity, cross-die wiring latency can be the bottleneck of low clock frequency. A simple heuristic is to place independent tasks (e.g., multi-head attentions) into different dies instead of executing with all resources to avoid cross-die communications. Since there is no data movement between these tasks, we also

do not add FIFOs between these tasks, which further reduces the cross-die wiring.

On-chip Memory Parallel Access Dimension. To serve multiple MAC units in each PE, scratchpad memory is partitioned based on access patterns. In INTAR, the PEA in the CCs may require different memory access patterns. For example, Figure 6 shows two dependent matrix multiply operations, with the dimension indicating the number of data accessed in parallel. The first tiled matrix multiply will compute 2048 MACs simultaneously ($4 \times 8 \times 64$) and the second matrix multiply computes 1024 MACs ($4 \times 4 \times 64$) if we align the parallel access pattern. Since we reuse the PEA across tasks, we need to align the throughput between tasks. Thus, it is necessary to further partition the inputs of the second matrix multiplication by two, causing high-fanout nets (HFN) at the write ports, increasing cycle time, and reducing the design frequency. To address this issue, we suggest tiling the operands such that the output tile has equal lengths at each dimension to align parallel read/write dimensions even after transposing, e.g., having 16×16 output tiles in the example.

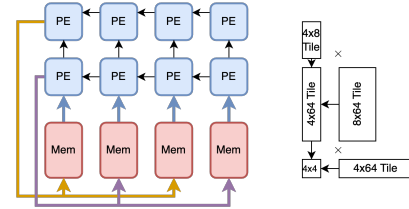


Fig. 6. Example of a design with high-fanout nets on write ports of on-chip memory banks due to unaligned parallel memory access dimensions.

To evaluate INTAR, we will show its broadness in DNN accelerations (Section V) and its advantages when deploying more complex DNNs on different FPGAs (Section VI).

V. EVALUATION 1: MULTI-TASK KERNELS IN HDV DNNs

A. Experiment Setup

To demonstrate the broadness of INTAR in HDV DNN accelerations, we construct a testbench with five multi-task kernels that can serve as a standalone DNN application (Multi-layer CNN, Variational Autoencoder) or participate in part of the DNN applications (Self Attention, FFN Layer, Gating Network). Table III illustrates these kernels in the evaluation. Unlike existing benchmarks [28], [44] for FPGA-based accelerator evaluation, our testbench has three features crucial for HDV: ① it covers various DNN applications in computer vision, language modeling, graph processing, etc., displayed in the "DNN Applications" column; ② it adopts parameters used in the real applications (e.g., Gating Network has the identical dimensionalities as Llama 2 [34]); and ③ kernels are all HDV, and we impose a memory constraint between the minimum and maximum input/output data sizes so that INTAR can exploit its ability to switch execution modes.

Using our testbench, we compare INTAR with human-optimized dataflow and sequential accelerators under the **same resource constraints**, including on-chip memory size, the

TABLE III

DESCRIPTIONS OF MULTI-TASK KERNELS USED IN EVALUATION 1 WITH THE CORRESPONDING PARAMETERS AND DATA SIZE CONFIGURATIONS.

Kernel	Description	DNN Applications	Parameters	Testbench Data Size Config	Data Variation Pattern
Self Attention (Attn)	A set of dependent matrix multiplications that extract the contextual relationships between tokens in a sequence.	Widely used in sequence modeling (Transformer [35], ViT [21], GAT [37])	256 token sequences. The hidden dimension is 1024.	Min data size: 0.5 MB, Max data size: 1.0 MB, On-chip memory constraint: 0.625 MB	Increase → Decrease → Increase → Decrease
FFN Layer (FFN)	Sequence of linear projections for feature extractions. Input is a single vector.	Elementary block in many CV and LLM applications (ResNet [22], YoloV3 [16], Transformer)	Input size = final output size = 256, First layer output size = 1024, second layer output size = 2048.	Min data size: 0.5 KB, Max data size: 2 KB, On-chip memory constraint: 1 KB	Increase → Increase → Decrease
Multi-layer CNN (M-CNN)	Sequence of convolutions with upsampling and pooling layers	Used in many CV applications (ResNet, VGG [36])	Input size = 224, kernel size = 3, 2 × 2 upsampling and pooling size.	Min data size: 98 KB, Max data size: 1.57 MB, On-chip memory constraint: 125 KB.	Increase → Increase → Decrease → Decrease
Variational Autoencoder (VAE)	Contains an encoder in convolutions for the latent space distribution and a decoder in transpose convolutions.	Used for image compression and the generator model in GAN (VAE-GAN [17])	Input size = 28, kernel sizes are 4 and 8, 2 channels and 2 filters	Min data size: 1.3 KB, Max data size: 3.1 KB, On-chip memory constraint: 1.5 KB	Decrease → Decrease → Increase → Increase
Gating Network (GN)	Two parallel linear projections with element-wise product and a sequential linear projection.	Llama-family LLMs [34]	Sequence length = 32, input dimension = 4096, hidden dimension = 11008	Min data size: 0.25 MB, Max data size: 0.67 MB, On-chip memory constraint: 0.5 MB	Increase → Decrease

number of DSPs, and off-chip memory bandwidth utilization. All designs are implemented utilizing Xilinx Vitis HLS 2021.2 with TAPA [19] and evaluated on Xilinx Alveo U280 FPGA board, with clock frequency at 300 MHz. We chose the human-optimized designs as the baseline since: ① There is a lack of existing designs of the kernels in our testbench with the same model and hardware configurations, and ② existing frameworks [6], [9], [15] for DNN application design generation on FPGAs do not handle off-chip memory communications or do not consider the extra resource constraints introduced to evaluate HDV DNNs.

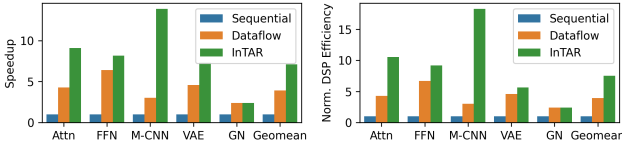


Fig. 7. Speedup and normalized DSP efficiency of InTAR over dataflow and sequential execution for the five multi-task kernels in the testbench.

B. Analysis

Figure 7 shows the speedup and DSP efficiency of InTAR over sequential and dataflow accelerators. Overall, InTAR achieves a speedup of $7.1\times$ and $1.8\times$ over sequential and dataflow accelerators, along with $7.5\times$ and $1.9\times$ higher DSP efficiency (GOP/s/DSP) in geometric mean. The performance boost of InTAR over sequential accelerators mainly comes from the reduction of off-chip memory access, where InTAR has 76% lower off-chip memory access volume than the sequential accelerators in geomean over the five kernels. For dataflow accelerators, InTAR is significantly faster in self-attention and multi-layer CNN than the other three kernels. There are two explanations. First, the two kernels mentioned have a higher data reuse between dependent tasks for matrix multiplications and convolutions, which requires data buffering and preprocessing before continuing the computations (e.g., the pooling layer of the multi-layer CNN will wait until producing two rows of outputs from the previous layer to downsample the data). Since the selected kernels have a long

chain of dependent tasks, pipeline stall latency may dominate the end-to-end latency. Second, InTAR can better reuse off-chip memory ports for these two kernels. For example, after loading inputs and finishing the first convolution layer in the multi-layer CNN, InTAR can utilize the memory ports allocated to the inputs to write outputs. Thus, InTAR has a higher effective off-chip read/write throughput than dataflow accelerators which only use the dedicated memory port for input/output. For Gating Networks, InTAR cannot further reduce latency compared with dataflow accelerators since only input and output data sizes are within the memory constraint and our schedule for InTAR is identical to pipelining all tasks.

VI. EVALUATION 2: GPT-2 INPUT PREFILLING

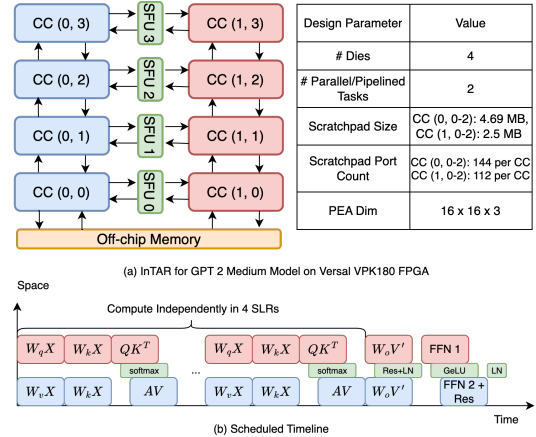


Fig. 8. A sample design of InTAR mapped to Versal VPK180 FPGA for GPT-2 Medium model. (a) Overall architecture and parameters. Each SLR contains two CCs and one SFU. (b) The scheduled timeline. The color of the blocks corresponds to the PEs or SFUs shown in (a).

A. Experiment Setup

We choose the GPT-2 medium input prefilling stage as the example of a complex DNN application to further evaluate InTAR and compare it with the corresponding SoTA accelerators. Figure 8(a) illustrates the architecture design for the GPT-2 medium model on the AMD Xilinx Versal VPK180

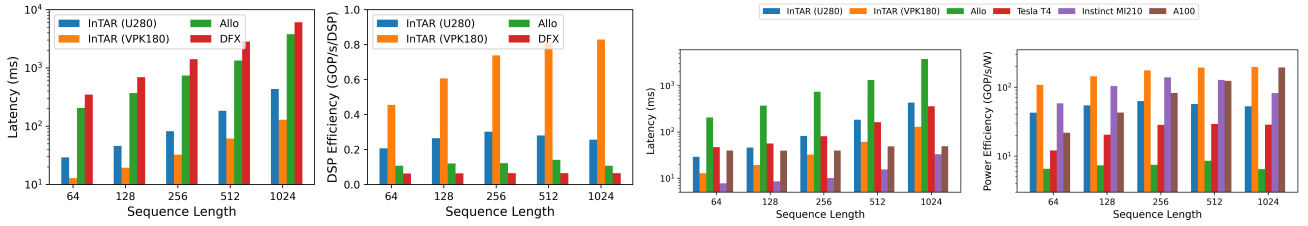


Fig. 9. Left: Latency and DSP efficiency of InTAR (U280, VPK180), Allo, and DFX. Both designs of InTAR are significantly more DSP efficient. Right: Latency and power efficiency of InTAR (U280, VPK180), Allo [9], and GPU solutions for GPT-2 medium model.

FPGA, based on the template in Section 2. The design has four rows of CCs spreading out to four SLRs of the FPGA. Each SLR includes two CCs and an SFU. Figure 8(b) depicts the GPT-2 medium schedule. Thanks to the grid structure of InTAR’s architecture template, we can adapt the design conveniently to other FPGA boards with slight modifications. We also implemented an InTAR design example for Alveo U280 FPGA, which contains three SLRs.

To generate the circuit design, we utilize Xilinx HLS with the TAPA framework [19] and prototype with the Vitis 2021.2 toolchain for U280 and Vitis 2024.1 for VPK180. The floorplanning of the CCs and SFUs is predetermined based on the architecture template and the rest of the modules (e.g., auxiliary buffers) are done by Autobridge [20]. The designs are both placed and routed for U280 and VPK180. We select Allo [9] and DFX [23] as the SoTA accelerators for the GPT-2 medium model to compare their throughput with InTAR.

TABLE IV
RESOURCE UTILIZATION AND FREQUENCY OF FPGA-BASED SOLUTIONS (ALLO, DFX, AND INTAR) FOR GPT-2 MEDIUM INPUT PREFILLING TASK. SPEEDUP IS NORMALIZED BASED ON DFX.

	Allo [9]	DFX [23]	InTAR	InTAR
Device	U280	U280	U280	VPK180
Frequency	247 MHz	200 MHz	224 MHz	300 MHz
BRAM	389 (19%)	1192 (59%)	535 (27%)	700 (14%)
DSP	1780 (20%)	3533 (39.2%)	6727 (75%)	6726 (47%)
LUT	569K (44%)	520K (40%)	485K (37%)	1074K (32%)
FF	653K (25%)	959K (43%)	627K (25%)	1072K (16%)
URAM	111 (12%)	104 (11%)	336 (35%)	412 (16%)
Norm. Speedup	1.83×	1.0×	14.64×	39.14×

Table IV lists the resource utilization and frequency. InTAR on VPK180 has lower DSP utilization than U280 since VPK180 has fewer cross-SLR wires than U280 and PEA sizes are highly correlated with cross-SLR communications. DFX is executed in FP16, and all other designs employ the W4A8 format. We scale the DSP efficiency for DFX to align the data type. For performance metrics, we use OpenCL profiling functions to get the latency and `xbutil` to measure the power within 100 runs on U280. Due to a lack of access to a physical device, we employ QEMU and the Xilinx Power Design Manager to calculate the latency and estimate the power consumption of VPK180. DFX is not included in comparing power efficiency due to a lack of data in the original work.

We also compare InTAR with various GPUs shown in Table V. PyTorch profiler measures the latency and memory transactions. To measure the power consumption, we employ the NVIDIA management library to probe the power every

10 ms and calculate the average power when it is stable. All GPUs are inference in BFloat16 format, which is a commonly supported and optimized data format for GPUs.

TABLE V
HARDWARE CONFIGURATIONS OF THE FPGAS AND GPUS

	U280	VPK180	T4	A100	MI210
Frequency	224 MHz	240 MHz	585 MHz	765 MHz	1.7 GHz
Bandwidth	460 GB/s	52.1 GB/s	320 GB/s	1.56 TB/s	1.64 TB/s
Max Power	75 W	180 W	70 W	250 W	300 W
Max Perf.	8.09 TOP/s	20.7 TOP/s	65.13 TOP/s	311.84 TOP/s	181 TOP/s
Process Node	TSMC 16nm	TSMC 7nm	TSMC 12nm	TSMC 7nm	TSMC 6nm

B. Analysis

Comparison with FPGA-based Accelerators. Figure 9 presents the latency, DSP efficiency, and power efficiency comparison between FPGA and GPU accelerators. Compared to Allo and DFX, InTAR on U280 is 7.99× and 14.64× faster, and 2.19× and 3.98× more DSP efficient, respectively. InTAR on VPK180 is 21.39× and 39.14× faster, and 5.66× and 10.44× more DSP efficient than Allo and DFX. InTAR on VPK180 is more DSP efficient than U280 since DSP58 has a higher throughput than DSP48. Additionally, implementing DSPs in dot-product modules on VPK180 trims the logic and further reduces cycles, leading to more than 2× boost in DSP efficiency.

Comparison with GPUs. As shown in Figure 9, InTAR on U280 achieves a 1.07× speedup in geometric mean over T4 and 2.41× speedup on VPK180. Especially for short sequences ($L \leq 256$), InTAR’s performance surpasses both T4 and A100 GPUs.

Moreover, with the same process node, InTAR on FPGAs attains higher power efficiency than GPUs. InTAR on U280 is 2.37× and 7.40× more efficient than NVIDIA T4 and Allo on U280. InTAR on VPK180 is 1.66× ~ 7.17× more efficient than T4, A100, MI210, and 22.4× than Allo. One source of latency and power overhead for GPUs is the off-chip memory access. Since GPUs execute tasks sequentially and GPT-2 medium tends to generate large intermediate data, off-chip memory access is more intense on GPUs than InTAR-optimized FPGA designs. As a result, InTAR has a 20% ~ 67% lower off-chip memory access compared to T4, A100, and MI210 after scaling to the same data format.

VII. CONCLUSION AND FUTURE WORK

In this work, we propose InTAR, a novel accelerator design paradigm for DNNs with high data volume variation. InTAR

enhances resource efficiency by switching execution patterns and performing model-specific optimizations. It surpasses SoTA FPGA accelerators in speed, DSP, and power efficiency, and, compared with GPUS, it reduces off-chip memory access.

While we are motivated and focused on DNNs, InTAR can potentially improve the performance of non-DNN HDV applications, which we plan to explore. Furthermore, future work including developing an optimized DSE engine to replace the heuristic-based scheduling and integrating InTAR into compilers are necessary to address InTAR's limitations.

REFERENCES

- [1] Alveo u280 data center accelerator card data sheet.
- [2] Amd versal hbm series product selection guide.
- [3] Stefan Abi-Karam, Yuqi He, Rishov Sarkar, Lakshmi Sathidevi, Zihang Qiao, and Cong Hao. Gengnn: A generic fpga framework for graph neural network acceleration. *arXiv preprint arXiv:2201.08475*, 2022.
- [4] Eunjin Baek, Dongup Kwon, and Jangwoo Kim. A multi-neural network acceleration architecture. In *2020 ACM/IEEE 47th Annual International Symposium on Computer Architecture (ISCA)*, pages 940–953. IEEE, 2020.
- [5] Yueyin Bai, Hao Zhou, Keqing Zhao, Hongji Wang, Jianli Chen, Jun Yu, and Kun Wang. Fet-opu: A flexible and efficient fpga-based overlay processor for transformer networks. In *2023 IEEE/ACM International Conference on Computer Aided Design (ICCAD)*, pages 1–9. IEEE, 2023.
- [6] Suhail Basalama, Atefeh Sohrabzadeh, Jie Wang, Licheng Guo, and Jason Cong. Flexcnn: An end-to-end framework for composing cnn accelerators on fpga. *ACM Transactions on Reconfigurable Technology and Systems*, 16(2):1–32, 2023.
- [7] Jingwei Cai, Yuchen Wei, Zuocong Wu, Sen Peng, and Kaisheng Ma. Inter-layer scheduling space definition and exploration for tiled accelerators. In *Proceedings of the 50th Annual International Symposium on Computer Architecture*, pages 1–17, 2023.
- [8] Hongzheng Chen, Jiahao Zhang, Yixiao Du, Shaojie Xiang, Zichao Yue, Niansong Zhang, Yaohui Cai, and Zhiru Zhang. Understanding the potential of fpga-based spatial acceleration for large language model inference. *ACM Transactions on Reconfigurable Technology and Systems*, 2024.
- [9] Hongzheng Chen, Niansong Zhang, Shaojie Xiang, Zhichen Zeng, Mengjia Dai, and Zhiru Zhang. Allo: A programming model for composable accelerator design. *Proceedings of the ACM on Programming Languages*, 8(PLDI):593–620, 2024.
- [10] Jason Cong, Hui Huang, Chiyuan Ma, Bingjun Xiao, and Peipei Zhou. A fully pipelined and dynamically composable architecture of cgra. In *2014 IEEE 22nd Annual International Symposium on Field-Programmable Custom Computing Machines*, pages 9–16. IEEE, 2014.
- [11] Jason Cong, Jason Lau, Gai Liu, Stephen Neuendorffer, Peichen Pan, Kees Vissers, and Zhiru Zhang. Fpga hls today: successes, challenges, and opportunities. *ACM Transactions on Reconfigurable Technology and Systems (TRETS)*, 15(4):1–42, 2022.
- [12] Jacob Devlin, Ming-Wei Chang, Kenton Lee, and Kristina Toutanova. Bert: Pre-training of deep bidirectional transformers for language understanding. *arXiv preprint arXiv:1810.04805*, 2018.
- [13] Li Dong, Nan Yang, Wenhui Wang, Furu Wei, Xiaodong Liu, Yu Wang, Jianfeng Gao, Ming Zhou, and Hsiao-Wuen Hon. Unified language model pre-training for natural language understanding and generation. *Advances in neural information processing systems*, 32, 2019.
- [14] Alexey Dosovitskiy, Lucas Beyer, Alexander Kolesnikov, Dirk Weissenborn, Xiaohua Zhai, Thomas Unterthiner, Mostafa Dehghani, Matthias Minderer, Georg Heigold, Sylvain Gelly, et al. An image is worth 16x16 words: Transformers for image recognition at scale. *arXiv preprint arXiv:2010.11929*, 2020.
- [15] Javier Duarte et al. Fast inference of deep neural networks in FPGAs for particle physics. *JINST*, 13(07):P07027, 2018.
- [16] Ali Farhadi and Joseph Redmon. Yolov3: An incremental improvement. In *Computer vision and pattern recognition*, volume 1804, pages 1–6. Springer Berlin/Heidelberg, Germany, 2018.
- [17] Rui Gao, Xingsong Hou, Jie Qin, Jiabin Chen, Li Liu, Fan Zhu, Zhao Zhang, and Ling Shao. Zero-vae-gan: Generating unseen features for generalized and transductive zero-shot learning. *IEEE Transactions on Image Processing*, 29:3665–3680, 2020.
- [18] David Gschwend. Zynqnet: An fpga-accelerated embedded convolutional neural network. *arXiv preprint arXiv:2005.06892*, 2020.
- [19] Licheng Guo, Yuze Chi, Jason Lau, Linghao Song, Xingyu Tian, Moazin Khatti, Weikang Qiao, Jie Wang, Ecenur Ustun, Zhenman Fang, et al. Tapa: a scalable task-parallel dataflow programming framework for modern fpgas with co-optimization of hls and physical design. *ACM Transactions on Reconfigurable Technology and Systems*, 16(4):1–31, 2023.
- [20] Licheng Guo, Yuze Chi, Jie Wang, Jason Lau, Weikang Qiao, Ecenur Ustun, Zhiru Zhang, and Jason Cong. Autobridge: Coupling coarse-grained floorplanning and pipelining for high-frequency hls design on multi-die fpgas. In *The 2021 ACM/SIGDA International Symposium on Field-Programmable Gate Arrays*, pages 81–92, 2021.
- [21] Kai Han, Yunhe Wang, Hanting Chen, Xinghao Chen, Jianyuan Guo, Zhenhua Liu, Yehui Tang, An Xiao, Chunjing Xu, Yixing Xu, et al. A survey on vision transformer. *IEEE transactions on pattern analysis and machine intelligence*, 45(1):87–110, 2022.
- [22] Kaiming He, Xiangyu Zhang, Shaoqing Ren, and Jian Sun. Deep residual learning for image recognition. In *Proceedings of the IEEE conference on computer vision and pattern recognition*, pages 770–778, 2016.
- [23] Seongmin Hong, Seungjae Moon, Junsoo Kim, Sungjae Lee, Minsub Kim, Dongsoo Lee, and Joo-Young Kim. Dfx: A low-latency multi-fpga appliance for accelerating transformer-based text generation. In *2022 55th IEEE/ACM International Symposium on Microarchitecture (MICRO)*, pages 616–630. IEEE, 2022.
- [24] Norm Jouppi, George Kurian, Sheng Li, Peter Ma, Rahul Nagarajan, Lifeng Nai, Nishant Patil, Suvinay Subramanian, Andy Swing, Brian Towles, et al. Tpu v4: An optically reconfigurable supercomputer for machine learning with hardware support for embeddings. In *Proceedings of the 50th Annual International Symposium on Computer Architecture*, pages 1–14, 2023.
- [25] Taeyoung Kong, Kalhan Koul, Priyanka Raina, Mark Horowitz, and Christopher Torng. Hardware abstractions and hardware mechanisms to support multi-task execution on coarse-grained reconfigurable arrays. *arXiv preprint arXiv:2301.00861*, 2023.
- [26] Sihao Liu, Jian Weng, Dylan Kupsh, Atefeh Sohrabzadeh, Zhengrong Wang, Licheng Guo, Jiuyang Liu, Maxim Zhulin, Rishabh Mani, Lucheng Zhang, et al. Overgen: Improving fpga usability through domain-specific overlay generation. In *2022 55th IEEE/ACM International Symposium on Microarchitecture (MICRO)*, pages 35–56. IEEE, 2022.
- [27] Zejian Liu, Gang Li, and Jian Cheng. Hardware acceleration of fully quantized bert for efficient natural language processing. In *2021 Design, Automation & Test in Europe Conference & Exhibition (DATE)*, pages 513–516. IEEE, 2021.
- [28] Louis-Noël Pouchet et al. Polybench: The polyhedral benchmark suite. URL: <http://www.cs.ucla.edu/pouchet/software/polybench>, 437:1–1, 2012.
- [29] Alec Radford, Jeffrey Wu, Rewon Child, David Luan, Dario Amodei, Ilya Sutskever, et al. Language models are unsupervised multitask learners. *OpenAI blog*, 1(8):9, 2019.
- [30] Mohaimenul Azam Khan Raiaan, Md Saddam Hossain Mukta, Kaniz Fatema, Nur Mohammad Fahad, Sadman Sakib, Most Marufatul Jannat Mim, Jubaer Ahmad, Mohammed Eunus Ali, and Sami Azam. A review on large language models: Architectures, applications, taxonomies, open issues and challenges. *IEEE Access*, 2024.
- [31] Masakazu Tanomoto, Shinya Takamaeda-Yamazaki, Jun Yao, and Yusuhiko Nakashima. A cgra-based approach for accelerating convolutional neural networks. In *2015 IEEE 9th International Symposium on Embedded Multicore/Many-core Systems-on-Chip*, pages 73–80. IEEE, 2015.
- [32] Ian Taras and Jason H Anderson. Impact of fpga architecture on area and performance of cgra overlays. In *2019 IEEE 27th Annual International Symposium on Field-Programmable Custom Computing Machines (FCCM)*, pages 87–95. IEEE, 2019.
- [33] Jianming Tong, Anirudh Itagi, Parsanth Chatarasi, and Tushar Krishna. Feather: A reconfigurable accelerator with data reordering support for low-cost on-chip dataflow switching. In *Proceedings of the 51th*

- Annual International Symposium on Computer Architecture, ISCA '24*, Argentina, 2024. Association for Computing Machinery.
- [34] Hugo Touvron, Louis Martin, Kevin Stone, Peter Albert, Amjad Almahairi, Yasmine Babaei, Nikolay Bashlykov, Soumya Batra, Prajjwal Bhargava, Shruti Bhosale, et al. Llama 2: Open foundation and fine-tuned chat models. *arXiv preprint arXiv:2307.09288*, 2023.
 - [35] Ashish Vaswani, Noam Shazeer, Niki Parmar, Jakob Uszkoreit, Llion Jones, Aidan N Gomez, Łukasz Kaiser, and Illia Polosukhin. Attention is all you need. *Advances in neural information processing systems*, 30, 2017.
 - [36] Andrea Vedaldi and Andrew Zisserman. Vgg convolutional neural networks practical. *Department of Engineering Science, University of Oxford*, 66, 2016.
 - [37] Petar Veličković, Guillem Cucurull, Arantxa Casanova, Adriana Romero, Pietro Lio, and Yoshua Bengio. Graph attention networks. *arXiv preprint arXiv:1710.10903*, 2017.
 - [38] Kizheppatt Vipin and Suhaib A Fahmy. Fpga dynamic and partial reconfiguration: A survey of architectures, methods, and applications. *ACM Computing Surveys (CSUR)*, 51(4):1–39, 2018.
 - [39] Saining Xie, Ross Girshick, Piotr Dollár, Zhuowen Tu, and Kaiming He. Aggregated residual transformations for deep neural networks. In *Proceedings of the IEEE conference on computer vision and pattern recognition*, pages 1492–1500, 2017.
 - [40] Yunxuan Yu, Chen Wu, Tiandong Zhao, Kun Wang, and Lei He. Opu: An fpga-based overlay processor for convolutional neural networks. *IEEE Transactions on Very Large Scale Integration (VLSI) Systems*, 28(1):35–47, 2019.
 - [41] Yunxuan Yu, Tiandong Zhao, Kun Wang, and Lei He. Light-opu: An fpga-based overlay processor for lightweight convolutional neural networks. In *Proceedings of the 2020 ACM/SIGDA International Symposium on Field-Programmable Gate Arrays*, pages 122–132, 2020.
 - [42] Shulin Zeng, Jun Liu, Guohao Dai, Xinhao Yang, Tianyu Fu, Hongyi Wang, Wenheng Ma, Hanbo Sun, Shiyao Li, Zixiao Huang, et al. Flightllm: Efficient large language model inference with a complete mapping flow on fpgas. In *Proceedings of the 2024 ACM/SIGDA International Symposium on Field Programmable Gate Arrays*, pages 223–234, 2024.
 - [43] Xiaofan Zhang, Hanchen Ye, Junsong Wang, Yonghua Lin, Jinjun Xiong, Wen-mei Hwu, and Deming Chen. Dnnexplorer: a framework for modeling and exploring a novel paradigm of fpga-based dnn accelerator. In *Proceedings of the 39th International Conference on Computer-Aided Design*, pages 1–9, 2020.
 - [44] Yuan Zhou, Udit Gupta, Steve Dai, Ritchie Zhao, Nitish Srivastava, Hanchen Jin, Joseph Featherston, Yi-Hsiang Lai, Gai Liu, Gustavo Angarita Velasquez, Wenping Wang, and Zhiru Zhang. Rosetta: A Realistic High-Level Synthesis Benchmark Suite for Software-Programmable FPGAs. *Int'l Symp. on Field-Programmable Gate Arrays (FPGA)*, Feb 2018.
 - [45] Jinming Zhuang, Zhuoping Yang, Shixin Ji, Heng Huang, Alex K Jones, Jingtong Hu, Yiyu Shi, and Peipei Zhou. Ssr: Spatial sequential hybrid architecture for latency throughput tradeoff in transformer acceleration. In *Proceedings of the 2024 ACM/SIGDA International Symposium on Field Programmable Gate Arrays*, pages 55–66, 2024.